

# Development and Breakdown of Görtler Vortices in High Speed Boundary Layers

Fei Li<sup>†</sup>, Meelan Choudhari<sup>&</sup>, Chau-Lyan Chang<sup>\*</sup>

*Computational AeroSciences Branch, NASA Langley Research Center, Hampton, VA 23681*

Minwei Wu<sup>#</sup>

*National Institute of Aerospace, Hampton, VA 23666*

Patrick T. Greene<sup>‡</sup>

*University of California, Los Angeles, CA 90095*

The nonlinear development of Görtler instability over a concave surface gives rise to a highly distorted stationary flow in the boundary layer that has strong velocity gradients in both spanwise and wall-normal directions. This distorted flow is susceptible to strong, high frequency secondary instability that leads to the onset of transition. For high Mach number flows, the boundary layer is also subject to the second mode instability. The nonlinear development of Görtler vortices and the ensuing growth and breakdown of secondary instability, the Görtler vortex interactions with second mode instabilities as well as oblique second mode interactions are examined in the context of both internal and external hypersonic configurations using nonlinear parabolized stability equations, 2-D eigenvalue analysis and direct numerical simulation. For Görtler vortex development inside the Purdue Mach 6 Ludwieg tube wind tunnel, multiple families of unstable secondary eigenmodes are identified and their linear and nonlinear evolution is examined. The computation of secondary instability is continued past the onset of transition to elucidate the physical mechanisms underlying the laminar breakdown process. Nonlinear breakdown scenarios associated with transition over a Mach 6 compression cone configuration are also explored.

## Nomenclature

$G_\theta$	Görtler number based on boundary layer momentum thickness
$R_\theta$	Reynolds number based on boundary layer momentum thickness
$T$	Temperature
$n$	Azimuthal wavenumber for axisymmetric configurations
$u$	Streamwise perturbation velocity
$\kappa^*$	Streamwise curvature of wall
$\lambda$	Spanwise or azimuthal wavelength
$\theta$	Momentum thickness of boundary layer
$\rho$	Density
$\omega_x$	Streamwise vorticity

---

<sup>†</sup> Aerospace Technologist, M.S. 128, fei.li@nasa.gov.

<sup>&</sup> Aerospace Technologist, M.S. 128, meelan.m.choudhari@nasa.gov, Associate Fellow AIAA.

<sup>\*</sup> Aerospace Technologist, M.S. 128, chau-lyan.chang@nasa.gov, Senior Member, AIAA.

<sup>#</sup> Research Scientist, minwei.wu@nianet.org.

<sup>‡</sup> Graduate student, Dept of Mech. and Aerospace Engineering, greene@seas.ucla.edu, Student Member AIAA.

## I. Introduction

Boundary-layer flow over a concave wall is subject to the Görtler instability, which is typically manifested in the form of counter-rotating pairs of stationary streamwise vortices. Regions of concave surface curvature occur in a number of technological applications across the speed regime. Subsonic and transonic applications include flow past turbine blades and supercritical airfoils designed for laminar flow control. In supersonic and hypersonic transition research, the Görtler instability becomes even more relevant as an important contributor to the onset of transition along the walls of high-speed wind tunnels<sup>1-3</sup> as well as along the forebody compression surface ahead of the engine inlet on scramjet vehicles<sup>4-5</sup>. Onset of transition along the tunnel walls leads to a substantial increase in the levels of free-stream disturbances encountered by wind tunnel models, compromising one's ability to simulate in-flight transition behavior on the models. On the other hand, it is desirable for the boundary layer to become turbulent ahead of the scramjet engine inlet, in which case the growth and breakdown of Görtler vortices could help achieve this goal without the added drag due to boundary layer trips.

Much of the previous research on the Görtler instability has been carried out in the context of low-speed flows; see, for instance, the reviews by Hall<sup>6</sup>, Saric<sup>7</sup> and Floryan<sup>8</sup>. Studies of Görtler instability in supersonic and hypersonic flows are limited to linear growth characteristics of primary waves<sup>9-13</sup>, with the exception of the high Reynolds number asymptotic theory by Fu and Hall<sup>14,15</sup> and computations of nonlinear interactions between second mode and Görtler instabilities<sup>16</sup>. The goal of this paper is to examine the nonlinear development of Görtler vortices in high-speed boundary layers, including their breakdown via high-frequency secondary instabilities and Görtler-second mode interactions.

An outline of this paper is as follows. Section II of this paper describes the flow configurations and the analysis codes used. Section III presents computational results for the large amplitude, primary Görtler instability. The linear secondary instability results are discussed in Section IV, nonlinear development and breakdown of the secondary instability are presented in Section V. Görtler and second mode interactions are described in Section VI. Oblique second mode interactions are discussed in Section VII and, finally, a summary of the paper is given in Section VIII.

## II. Flow Configuration and Analysis Codes

The first flow configuration examined herein corresponds to that of the Boeing/AFOSR Mach 6 wind tunnel at Purdue University<sup>3</sup>, which has a circular test section with a diameter of 9.5 inches. The steady axisymmetric flow field inside the Ludwig tube is computed using a high order DNS code<sup>17</sup> with a grid of 800 by 800 in the streamwise and radial directions for a case with a stagnation pressure of 896.3 kPa, a stagnation temperature of 433 K and a unit Reynolds number of approximately  $9.9 \times 10^6$  per meter<sup>17</sup>. The computational domain starts at 0.27 meters upstream of the throat and ends at 2.58 meters downstream of the throat. Between the throat and the tunnel test section, there exists a long portion of concave surface and the growth of Görtler vortices over this region will have a direct impact on the flow quality in the tunnel. For this configuration, the current study concentrates on the transition route via the secondary instability mechanism.

To study the generic features of transition within the nozzle wall boundary layer, the surface temperature is assumed to correspond to adiabatic surface conditions. The actual temperature distribution along the nozzle surface has never been measured. However, an estimated temperature distribution is reported by Schneider *et al.*<sup>18</sup>. The relatively modest differences between the reported temperature distribution and the adiabatic temperature distribution are not expected to produce a major impact on the Görtler vortex evolution and, in particular, the breakdown scenario associated with high-frequency secondary instabilities.

The second flow configuration is the Purdue Mach 6 compression cone<sup>19</sup> with a stagnation pressure of 930.1 kPa, a stagnation temperature of 766.8 K, and unit Reynolds number of  $10.2 \times 10^6$  per meter. The surface of the cone is 0.47 meters long with a constant radius of curvature equal to 3 meters and tangentially joins a small nose sphere of radius 0.16 mm at an initial half-angle of 1.4 degrees. The steady axisymmetric flow over the cone is computed by VULCAN<sup>20</sup> - a Navier-Stokes solver, using a grid of 2241 by 385 points in the streamwise and wall-normal directions, respectively. The boundary layer over this surface is susceptible to moderate Görtler instability as well as

strong second mode instability. For this compression cone configuration, the current study is focused on the transition route via interactions between the Görtler mode and the second mode.

Linear and nonlinear development of the Görtler instability modes is computed using parabolized stability equations (PSE) as implemented in the Langley Stability and Transition Analysis Code(s) (LASTRAC)<sup>21</sup>. Linear growth characteristics of secondary instability modes are predicted using the methodology outlined by Li and Choudhari<sup>22</sup>. DNS of nonlinear evolution of secondary instability is performed using a high order flow solver based on 7<sup>th</sup> order WENO scheme for the convective flux terms<sup>23</sup>. Although not discussed herein, selected computations using all three tools (DNS, PSE, and secondary instability) have been verified for grid convergence.

In addition to the Mach 6 tunnel flow field and the Mach 6 compression cone, a flat plate configuration is used for studying the development of Görtler vortices. This configuration is used because a flat-plate flow is one of the simplest boundary-layer flows and has a similarity solution. These properties make it easier to carry out parametric studies.

A relevant non-dimensional quantity in problems involving the Görtler instability is the Görtler number defined as

$$G_\theta = R_\theta (\theta \kappa^*)^{1/2} \quad (1)$$

where  $\theta$  is the boundary layer displacement thickness,  $R_\theta$  is the Reynolds number based on displacement thickness and  $\kappa^*$  is the dimensional surface curvature. In general, as the Görtler number increases, Görtler vortices become more unstable. In the limit of large Reynolds number and small surface curvature at a fixed value of the Görtler number, the leading order boundary layer solution is not affected by the curvature of the plate and is the same as that for a flat plate (see *e.g.* Spall and Malik<sup>9</sup>). This ensures the validity of using the flat plate similarity solution for the Görtler problem.

### III. Nonlinear Development of Görtler Vortices

Linear stability calculations show that the azimuthal wavenumber of  $n=100$  (i.e., 100 vortices across the wind tunnel circumference) corresponds, approximately, to the highest linear amplification of stationary Görtler vortices for the Mach 6 wind tunnel case. The nonlinear development of this mode, which has a spanwise wavelength of  $\lambda \approx 7.6\text{mm}$  within the test section, is computed via nonlinear PSE for a range of initial amplitudes, starting at 0.67 meters downstream of the wind-tunnel throat where the  $n=100$  mode first becomes linearly unstable .

Computational results with an initial temperature perturbation corresponding to 1% of the free-stream temperature are shown in Figure 1, which illustrates representative contours of streamwise velocity, and temperature distributions along with the derivatives of the streamwise velocity in the wall-normal and spanwise directions at selected streamwise locations. Up to the onset of nonlinear saturation of the Görtler vortices, the mushroom shaped structures usually associated with finite amplitude Görtler vortices (e.g., Hall and Horseman<sup>24</sup>, Li and Malik<sup>25</sup> and Whang and Zhong<sup>16</sup> for nonlinear Gortler instability in low-speed and hypersonic flows, respectively ), are not seen in the present case. Instead, the nonlinear development of the counter-rotating vortex pair associated with Gortler modes gives rise to bell-shaped structures as depicted in Fig. 1 (a) and (b). Scrutiny of the velocity derivatives in the cross-planes shows that strong velocity gradients exist in the boundary layer flow modified by the finite amplitude Görtler vortices (Figures 1 (c) and (d)). In-plane streamlines are shown in Figure 1 (e) in a slightly tilted cross-plane in order to account for the fact the axis of the Görtler vortex is not quite parallel to the wall as a result of the streamwise amplification of the Görtler vortices. The pair of counter-rotating vortices brings up low speed fluid up from the wall and, on either side, pushes the high speed fluid down toward the wall. This process results in strongly non-uniform velocity profiles across the span.

Nonlinear evolution of Görtler vortices was also computed for a similarity boundary layer over a concave plate with a constant radius of curvature of 20 meters. In this case, the most amplified mode has a spanwise wavelength of approximately 8 mm and computations were carried out for three cases with spanwise wavelengths of 4, 8, and 16 mm. The streamwise velocity contours at streamwise locations where the nonlinear Görtler vortices are nearly saturated are shown in Figure 1 (f). It can be seen that, in all three cases, the bell-shaped features persist up to the saturation of vortex amplitudes. The well-known mushroom shaped contours are observed farther downstream (i.e.,

well into the region of saturation), as shown by the DNS computations. The Görtler vortex modes were seeded via a specified roughness near the neutral point of the vortex mode. Figure 1 (g) shows the mushroom structures at  $X = 2$  and  $2.2$  m with the onset of nonlinear saturation at approximately  $1.9$  m.

The secondary instability examined in Hall and Horseman<sup>24</sup> and Li and Malik<sup>25</sup> for low speed flows all ride on the edge of the mushroom structure. As will be shown later, strong secondary instability can also be sustained by the precursor bell shaped structures, even without the presence of the usual mushroom-structure.

In crossflow dominated boundary-layer flows over swept wings, a mechanism for delaying transition exists whereby a sub-dominant crossflow mode that is less likely to cause transition is artificially introduced with moderate initial amplitude, resulting in a growth reduction of the most dangerous, dominant crossflow mode (see Saric *et al.*<sup>26</sup> and Li *et al.*<sup>27</sup>). Despite the differences between the physical origin of the crossflow and Görtler instabilities, it is tempting to investigate whether a similar mechanism might possibly apply to the Görtler vortices as well. To this end, a series of computations were carried out, in which the initial amplitude of the dominant mode of azimuthal wavenumber 100 is kept fixed at a small value while a sub-dominant mode of azimuthal wavenumber 200 is introduced at various large initial amplitudes. Figure 2 shows the development of modal amplitudes of the respective modes. Despite the large variations in initial amplitudes of the sub-dominant control mode, the target mode is nearly unaffected, suggesting that this control methodology may not be effective in boundary layer flow dominated by Görtler vortex instability. In the crossflow case, the instability is primarily due to the existence of an inflection point in the three-dimensional boundary layer profile. The growth of the sub-dominant mode modifies the boundary layer and the dominant mode is thus affected. In the Görtler case, the instability is mainly due to a centrifugal mechanism associated with the concave wall. The introduction of the sub-dominant mode obviously does not modify the wall curvature and, therefore, is unlikely to affect the dominant mode in a major way.

#### IV. Linear Secondary Instability

Nonlinear Görtler vortices such as those presented in Figure 1 lead to inflectional profiles in both wall-normal and spanwise directions. As such, they are susceptible to various families of high frequency secondary instability, which have previously been studied in the context of incompressible flows using simplified, inviscid secondary instability models<sup>24, 25</sup>. In the current research, secondary instability of Görtler vortices in high speed boundary layers is studied using a fully viscous, spatial stability model that has been used to compute secondary instability of crossflow vortices<sup>22</sup>. In particular, a Görtler mode of spanwise wavenumber  $n = 100$  and an initial velocity amplitude of  $1.8 \times 10^{-3}$  is chosen to be the base flow for secondary instability in the Purdue wind tunnel case. This mode develops and barely reaches saturation at the end of the computational domain ( $X = 2.58$  m).

For the Görtler vortices in the Purdue wind tunnel case, three families of unstable secondary instabilities have been identified. These are designated modes 1 through 3, of which only mode 1 has a large enough growth rate and long enough range of growth region to achieve appreciable values of N-factor. In Figure 3 (a), modes 1 and 2 are represented by red and green colors, respectively. Each line corresponds to a different frequency. The frequency of the instability modes that achieves the largest N-factors for both families is approximately 53 kHz. An N-factor of 9 is reached by mode 1 approximately 2.57 meters downstream of the throat after becoming unstable at approximately 2.00 meters. Figure 3 (b) shows the spatial growth rate curves of the three families as functions of downstream distance. Figure 3 (c) shows the spatial growth rate versus frequency for all three families at a distance of 2.5 meters downstream of the throat. It is seen that the most unstable family corresponding to mode 1 extends over a frequency range of approximately 0 to 100 kHz. The mode shapes for all three families at 2.5 meters are shown in Figure 4, which would correspond to the root-mean-square values mapped out by some probe traversing the same streamwise plane. The most unstable family (mode 1) is anti-symmetric with respect to the vertical symmetry line between a pair of counter-rotating Görtler vortices in the sense that the streamwise and wall-normal velocity fluctuations and the temperature fluctuation on the two sides are 180 degrees out of phase, whereas modes 2 and 3 are symmetric modes. It can be seen, by examining the contour legends in Figure 4, that the secondary instability is dominated by large temperature fluctuations for all three modes, in contrast to corresponding low Mach number cases where velocity fluctuations dominate.

## V. Breakdown of Secondary Instability

The linear secondary instability results described above are only valid as long as the amplitude of the secondary modes remains sufficiently small. Since the growth of the secondary modes is quite rapid, a secondary N-factor criterion similar to that used in previous work<sup>27</sup> related to crossflow instability may be used for transition onset prediction. However, to gain additional insights into the nature of Görtler vortex breakdown associated with the nonlinear development of the secondary instability modes (and, hence, to predict the onset of transition in a more rational fashion), both PSE and direct numerical simulations (DNS) are used to extend the computation into the breakdown region. PSE can be used, at least, up to the earlier stages of breakdown, at a computational expense that is orders of magnitude less than the DNS. The applicability of PSE for this purpose has been demonstrated for incompressible Görtler vortex computations<sup>25</sup> and compressible crossflow vortex computations<sup>27</sup>. This methodology can also be applied to elucidate the breakdown mechanisms for the present case of Görtler vortices in a high-speed boundary layer.

The most unstable secondary instability mode of 52.5 kHz for the wind tunnel configuration is simulated via nonlinear PSE by imposing its eigenfunction near the neutral point as part of the initial condition in addition to the steady primary Görtler modes. Its nonlinear development is traced downstream for different initial amplitudes. Modal amplitudes of the secondary instability as well as those of the steady Görtler modes are shown in Figure 5 using green and red lines, respectively. The amplitudes of secondary instability modes as predicted by the linear theory discussed in Section IV are shown via black dots. Given that the PSE solution accounts for both nonparallel and surface curvature effects and the linear theory ignores both, the agreement between the PSE results and the linear theory predictions is very good over considerable distances from the neutral point. At even larger distances from the neutral point, the two sets of predictions begin to depart from each other as a result of the increasing significance of nonlinear effects which are only accounted for in the PSE predictions.

Figure 6 shows the RMS value of streamwise velocity fluctuations at two streamwise planes, one at a small distance from the neutral point where the disturbance amplitude is small and another at a larger distance where nonlinear effects are strong. The RMS contours look very similar to the eigenfunctions shown in Figure 4 (a). The RMS contours shown on the right of the Figure 6 appear “fatter” compared with those shown on the left, a strong indication of the nonlinear effects at play.

To carry the simulation well into the breakdown region, DNS is employed. The sequence of images in Figure 7 illustrates how the cross plane contours of mean and fluctuating u-velocity evolve during the breakdown induced by the high-frequency secondary instability. The spanwise extent of each image corresponds to a single azimuthal wavelength of the primary Görtler mode. When the disturbance motion is dominated by the primary Görtler vortex, *i.e.* the high-frequency secondary instability is weak, the initially sinusoidal mean velocity contours steepen to acquire a bell-shaped structure, with the top of this bell projecting farther out with increasing downstream distance. This is consistent with the nonlinear PSE results shown in Figure 1. However, the increasingly stronger Reynolds stresses associated with the high-frequency secondary instability eventually lead to visible distortion of the bell contours. Specifically, the region of high wall-normal shear near the center of each cross-section begins to move closer to the wall, and is accompanied by the emergence of a pair of high-shear regions near the outer ends. The highest velocity fluctuations are associated with the center peak and the location where they occur migrates closer to the wall as the breakdown progresses.

The anti-symmetric secondary instability mode causes the Görtler vortex structure to display sinuous motions and is termed the “sinuous mode” in by Swearingen and Blackwelder.<sup>28</sup> In the left of Figure 8, it is seen that the instantaneous iso-surface of streamwise velocity component shows the sinuous oscillations of the primary Görtler vortices and those oscillations lead to a pair of high gradient regions on the flanks, with the centerline peak moving downward, as we noted in the context of mean and fluctuating u contours (Figure 7). The instantaneous u contours close to the centerline plane are shown in the center of Figure 8, and reveal the azimuthal spreading of fluctuations towards the center plane. The streamwise evolution of wall shear for inflow secondary instability amplitudes varying over a 6-fold range are shown in Figure 9, indicating the distinct and monotonically upstream movement in transition onset as a function of the facility disturbance environment. Correlation of transition onset location with the absolute local amplitude of secondary instability is currently being investigated.

## VI. Breakdown via Görtler and Second Mode Interactions

For hypersonic boundary layers, second mode instability can be a significant factor leading to transition. In the case of the compression cone described in Section II, the most amplified second mode has an azimuthal wavenumber of  $n = 0$  and a frequency of approximately 300 kHz. Since the boundary layer over the compression cone also supports Görtler instability because of the concave longitudinal curvature, interactions between the Görtler vortices and the second mode waves provide another likely path for the onset of transition. Results pertaining to oblique mode interactions are presented in Section VII below. Here, it suffices to mention that the interaction between a pair of oblique non-stationary waves generates longitudinal stationary vortex modes that grow rather rapidly as the flow approaches the onset of transition. Thus, the concave surface curvature that destabilizes the Görtler instability also plays a role during the oblique mode interactions.

Figure 10 shows the linear N-factors of both the Görtler modes and the second modes. The most amplified Görtler mode has an azimuthal wavenumber of approximately  $n=50$ , for which the maximum N-factor at the end of the cone is just under 6 (Figure 10 (a)). Amplification characteristics of axisymmetric (i.e.,  $n=0$ ) second mode disturbances of various frequencies are shown in Figure 10 (b). Disturbance frequencies in the vicinity of 300 kHz attain the highest N-factors values over the length of the cone. Figure 10(c) shows the N-factors of oblique second modes at a fixed frequency of 300 kHz. Observe that an N-factor of 10 is reached even for the relatively oblique second mode disturbance with an azimuthal wavenumber of  $n=24$ .

As discussed previously, the process of laminar breakdown via interactions between the Görtler mode and second mode instabilities was studied for the compression cone boundary layer. Using nonlinear PSE, the most amplified Görtler mode with  $n = 50$  and the most amplified (i.e., axisymmetric) second mode wave with a frequency of 300 kHz are initiated at  $x = 0.097$  m. Two initial amplitudes of the Görtler mode are considered, namely,  $10^{-2}$  and  $10^{-3}$ , in combination with three initial amplitudes for the second mode wave, namely  $10^{-5}$ ,  $10^{-4}$  and  $10^{-3}$ , for a total of six different computations.

Figure 11 shows the nonlinear co-evolution of the Görtler and second modes. Initially, the modal amplitudes of the two different types of instabilities appear to evolve independently of each other. That is, the modal evolution of each mode type would, by and large, be unaltered if the other type of instability were absent. As both types of modes gain in amplitudes, the monotonic but slow evolution gives way to relatively more rapid variations, indicating strong interactions between the two instabilities (Figure 11 (a)). A typical characteristic of the onset of transition is the rapid rise in wall shear, which may be observed in Figure 11 (b) for all selected combinations of the initial amplitudes of the Görtler vortex and second mode wave. If the streamwise location where the wall shear begins to rise is used as the measure of transition onset location, one finds that a 10-fold reduction in the second mode initial amplitude would delay the onset of transition by approximately 0.03 meters (or approximately 6.4 percent of the cone length). For the weakest Görtler-second mode combination of initial amplitudes  $10^{-3}$  and  $10^{-5}$ , respectively, the transition onset is at  $X = 0.26$  meters.

## VII. Breakdown via Oblique Second Mode Interactions

As previously discussed in the context of Figure 10 (c), oblique second mode waves are linearly less unstable than the axisymmetric second mode waves. Nonetheless, the peak N-factors associated the oblique modes can be quite large. For example, second mode waves with a spanwise wavenumber  $n=24$  achieve an N-factor of nearly 10 near the end of the cone model. Interactions between pairs of oblique waves with equal amplitude, but opposite orientations (e.g.,  $n=\pm 24$ ) constitutes an additional transition mechanism for the compression cone. Oblique wave interactions between  $n=\pm 24$  waves will generate strong stationary longitudinal vortices with  $n=48$ , which are analogous to the linearly most unstable stationary Görtler mode. The scenario of oblique second mode interactions is investigated here using nonlinear PSE with five different initial amplitudes, namely,  $10^{-6}$ ,  $10^{-5}$ ,  $10^{-4}$ ,  $10^{-3}$  and  $10^{-2}$ .

Unlike the 2D second mode ( $n=0$ ), which becomes unstable at approximately  $X = 0.1$  meters, the oblique secondary mode of wavenumber  $n=24$  does not become unstable until approximately  $X = 0.2$  meters. In the case of the strongest pair of oblique waves with an initial amplitude of  $10^{-2}$ , transition onset based on the rise in wall mean shear corresponds to  $X \approx 0.25$  meters (Fig. 12). However, even the weakest combination of Görtler vortex and axisymmetric second mode from Section VI could have produced transition onset at approximately the same

location . Therefore, as long as the surface roughness can lead to modest excitation of stationary Görtler modes, transition via oblique second mode interactions at a frequency of 300 kHz appears to be a less likely scenario than the interactions between Görtler vortices and the axisymmetric second mode. Essentially, the oblique second mode has too low a growth rate compared with its 2D counterpart and, furthermore, this weaker growth begins too late (at approximately  $X = 0.2$  meters) for the resulting stationary vortex mode to help precipitate an earlier transition via oblique mode breakdown..

Another potential mechanism for transition over the compression cone corresponds to the breakdown of secondary instability of large amplitude 2D second mode. However, this scenario, which does not involve the Görtler instability, is beyond the scope of the present paper, and will be reported in a future paper.

### **VIII. Summary**

The linear and nonlinear growth of Görtler instability in hypersonic boundary layers and the associated transition mechanisms are studied using a combination of PSE, 2-D eigenvalue analysis, and DNS. One of the model flows corresponds to a Mach 6 wind tunnel whose concave wall between the throat and the test section leads to Görtler instability.

Linear stability results show that the most amplified primary Görtler mode has an azimuthal wavenumber of approximately  $n=100$ . Nonlinear evolution of this mode leads to distinct bell-shaped structures, which can sustain strong enough secondary instabilities to cause the onset of transition. The most unstable linear secondary instability mode is anti-symmetric with respect to the line of symmetry of the Görtler vortices. It first becomes unstable at a distance of approximately 2 meters downstream of the wind tunnel throat and reaches a N-factor of 9 at approximately 2.57 meters.

As the anti-symmetric secondary instability mode develops downstream, nonlinear effects set in, which at first, give rise to sinuous motions of the Görtler vortices. Eventually, with higher harmonics of the secondary instability becoming significant, the bell structures of primary Görtler vortices disappear and the unsteady fluctuations move progressively closer to the wall, leading to a rise in the mean wall shear as transition proceeds.

Potential control of dominant Görtler modes via the introduction of subdominant modes with a larger initial amplitude was investigated. It was shown that the dominant mode evolution is, by and large, unaffected by the presence of the subdominant mode. The reason for the ineffectiveness of such a control mechanism is that the existence of the Görtler instability is associated with the concave wall curvature, which is unaffected by this control technique. Interactions with the other modes and/or the basic state modification associated with them have a relatively small influence on the growth of the dominant node.

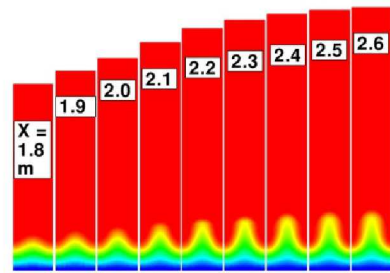
An additional mechanism for transition in hypersonic boundary layers involving concave surface curvature is that of nonlinear interactions between Görtler and second mode instabilities as demonstrated by computations for the compressible cone case. Other transition mechanisms relevant to this case include the oblique mode breakdown due to relatively less unstable, oblique, second mode instabilities and the fundamental and subharmonic secondary instabilities of the dominant, axisymmetric second mode. Which one of these scenarios is most relevant in any given case will depend on the environmental disturbances and the receptivity characteristics of the model. Receptivity to natural surface roughness and its influence on the transition mechanisms will be addressed in a follow-on paper.

### **Acknowledgments**

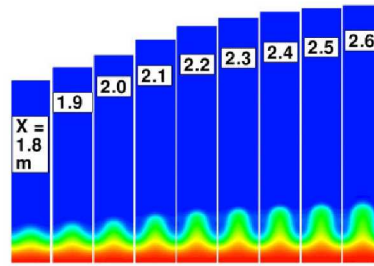
The authors would like to thank Prof. S.P. Schneider and his research group at Purdue University for technical communications related to their quiet tunnel facility and the compression cone configuration. Assistance by Mr. Jeff White during mean-flow calculations for the compression cone configuration is also appreciated.

## References

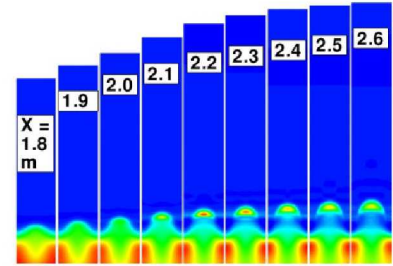
1. Beckwith, I. E., Malik, M. R., Chen F.-J. and Bushnell, D. M. "Effects of nozzle design parameters on the extent of quiet test flow at Mach 3.5," *IUTAM Symp. On Laminar-Turbulent Transition, Novosibirsk, USSR (ed. V.V. Kozlov)*, pp. 589-600, 1984.
2. Chen, F. J., Malik, M. R. and Beckwith, I. E. "Görtler Instability and Supersonic Quiet Nozzle Design," *AIAA J.*, Vol. 30, No. 8, August 1992.
3. Schneider, S.P., "Design of a Mach-6 Quiet-Flow Wind-Tunnel Nozzle using the e\*\*N Method for Transition Estimation," AIAA Paper 1998-0546, 1998.
4. Schneider, S.P., "Hypersonic Laminar-Turbulent Transition on Circular Cones and Scramjet Forebodies," *Progress in Aerospace Sciences*, Vol. 40, no. 1-2, Jan-Feb. 2004, pp. 1-50.
5. Choudhari, M. M, Li, F. and Edwards, J. E., "Stability analysis of roughness array wake in a high-speed boundary layer," AIAA Paper 2009-0170, 2009.
6. Hall, P., "Görtler vortices in growing boundary layers: the leading edge receptivity problem, linear growth, and nonlinear breakdown stage," *Mathematika*, Vol. 37, pp. 151-189, 1990.
7. Saric, W. S., "Görtler vortices," 1994, *Ann. Rev. Fluid Mech.*, Vol. 26, pp. 379-409, 1991.
8. Floryan, J. M., "On the Görtler vortex instability of boundary layers," *Prog. Aerospace Sci.*, Vol. 28, pp 235-271, 1992.
9. Spall, R. E. and Malik, M. R., "Görtler Vortices in Supersonic and Hypersonic Boundary Layers," *Phys. Fluids A*, Vol. 1, No. 11, p. 1822, November 1989.
10. Hall, P. and Malik, M. R., "The Growth of Görtler Vortices in Compressible Boundary Layers," *J. Engineering Mathematics*, Vol. 23, No. 3, pp. 239-252, September 1989.
11. Hall, P. and Fu, Y.B., "The Görtler vortex instability mechanism in hypersonic boundary layers," *J. Theor. Comp. Fluid Mechanics*, Vol. 3, pp. 125-134, 1989.
12. Fu, Y., Hall, P. and Blackaby, N., "On the Görtler vortex instability of a Sutherland Law fluid," *Phil. Trans. Roy. Soc. A.*, Vol. 342, pp. 325-377, 1992.
13. Fu, Y. and Hall, P., "The effect of crossflow on the instability of hypersonic boundary layers," *J. Fluid Mech.*, Vol. 276, 343-367, 1993.
14. Fu, Y. and Hall, P., "Nonlinear development and secondary instability of large amplitude Görtler vortices in hypersonic boundary layers," *Euro. J. Mech. B Fluids*, Vol. 11, pp. 1-46, 1992.
15. Fu, Y. and Hall, P., "Effects of Görtler vortices, wallcooling, gas dissociation on the Rayleigh instability in a hypersonic boundary layer," *J. Fluid Mech.*, Vol. 247, pp. 503-525, 1993.
16. Whang, C. W. and Zhong, X., "Nonlinear Interaction of Görtler and Second Shear Modes in Hypersonic Boundary-Layers," AIAA Paper 2000-0536, 2000.
17. Greene, P. T., Eldredge J. D., Zhong X. and Kim, J., "A Numerical Study of Purdue Mach 6 Tunnel with a Roughness Elements," AIAA Paper 2009-174, 2009.
18. Schneider, S.P., Rufer, S.J., Randall, L., and Skoch, C., "Shakedown of the Purdue Mach-6 Quiet-Flow Ludwig Tube," AIAA Paper 2001-0457, 2001.
19. Wheaton, B. M., Juliano, T. J., Berridge, D. C., Chou, A., Gilbert, P. L., Casper, K. M., Sheen, L. E. and Schneider, S. P., "Instability and Transition Measurements in the Mach-6 Quiet Tunnel," AIAA Paper 2009-3559, 2009.
20. <http://vulcan-cfd.larc.nasa.gov/index.html>
21. Chang, C.-L., "Langley Stability and Transition Analysis Code (LASTRAC) Version 1.2 User Manual," *NASA/TM-2004-213233*, 2004.
22. Li, F. and Choudhari, M., "Spatially Developing Secondary Instabilities and Attachment Line Instability in Supersonic Boundary Layers," AIAA Paper 2008-590, 2008.
23. Martin, M. P., Taylor, E. M., Wu, M., and Weirs, V. G., "A Bandwidth-optimized WENO Scheme for the Effective Direct Numerical Simulation of Compressible Turbulence," *J. Comp. Physics*, Vol. 220, pp. 270-289, 2006.
24. Hall, P., and Horseman, N. J., "The linear Inviscid Secondary Instability of Longitudinal Vortex Structures in Boundary Layers," *J. Fluid Mech.*, Vol. 232, pp. 357-375, 1991.
25. Li, F. and Malik, M. R. "Fundamental and Subharmonic Secondary Instabilities of Görtler Vortices," *J. Fluid Mech.*, Vol. 297, pp. 77-100, 1995.
26. Saric, W. S., Carillo, R. B., and Reibert, M. S., "Leading Edge Roughness as a Transition Control Mechanism," AIAA Paper 98-0781, 1998.
27. Li, F., Choudhari, M. M., Chang, C.-L., Streett, C. L. and Carpenter, M. H., "Roughness Based Crossflow Transition Control: A Computational Assessment," AIAA Paper 2009-4105, 2009.
28. Swearingen, J. D. and Blackwelder, R. F., "The Growth and Breakdown of Streamwise Vortices in the Presence of a Wall," *J. Fluid Mech.* Vol. 182, pp 255-290, 1987.



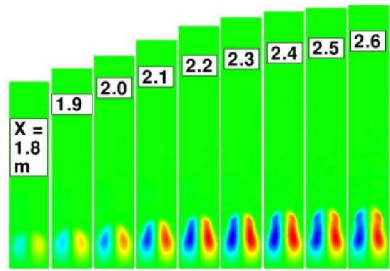
(a) Streamwise velocity  $u$ .



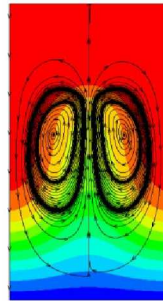
(b) Temperature.



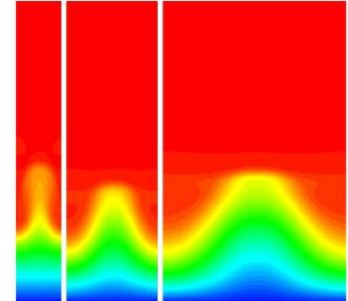
(c) Wall normal velocity gradient of streamwise velocity.



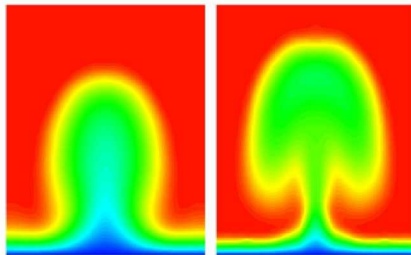
(d) Spanwise gradient of streamwise velocity.



(e) In-plane streamlines.



(f) Streamwise velocity for 4, 8 and 16 mm spanwise wavelength on a curved plate.



(g) Mushroom structures of a curved plate in nonlinear saturation region of Görtler vortices (8 mm). Left :  $X = 2.0$  m ; right :  $X = 2.2$  m. Onset of saturation at 1.9 m.

Figure 1. Nonlinear development of Görtler vortices. Contours of streamwise velocity, temperature and velocity derivatives in cross-planes at selected streamwise stations with circumferential wave number of the finite-amplitude Görtler vortices corresponding to  $n = 100$  ((a) – (d)), in-plane streamlines (e), streamwise velocity contours for various spanwise wavelengths on a curved plate (f) and (g).

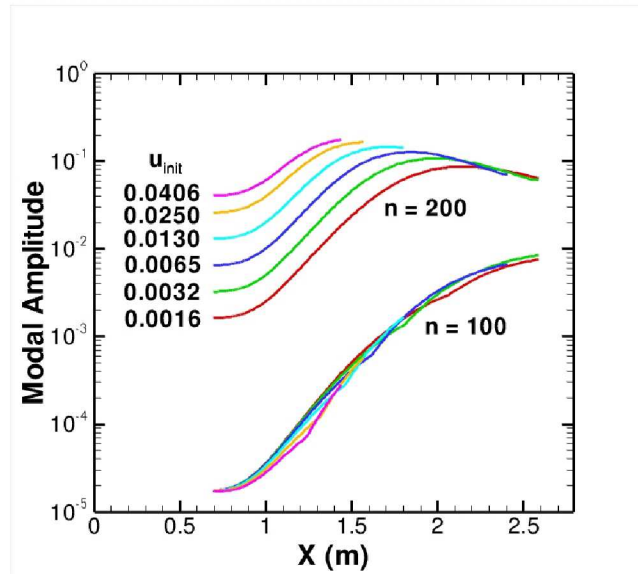
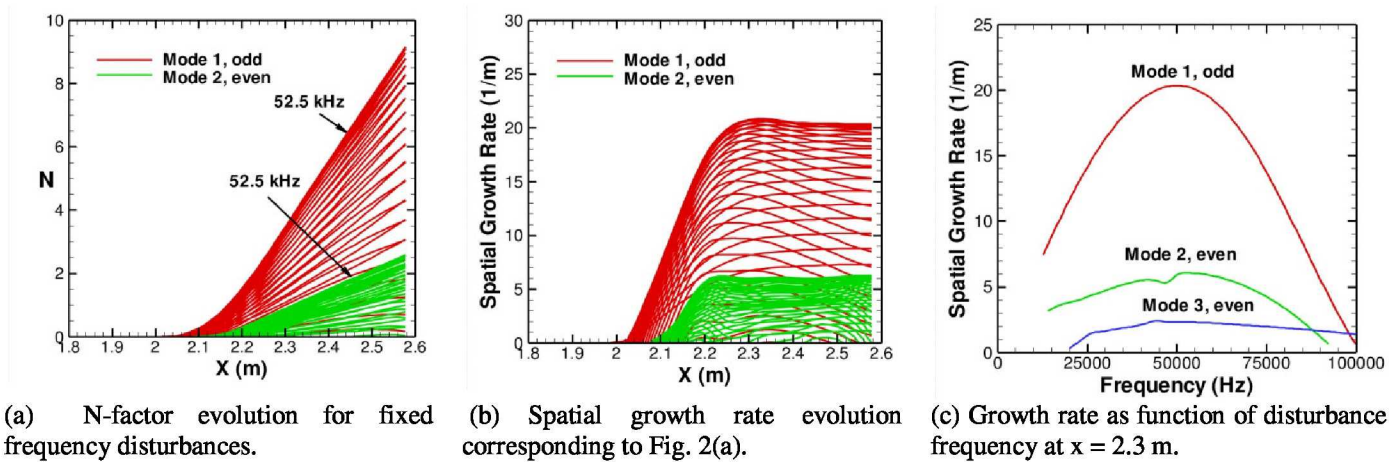


Figure 2. Effect of introducing less unstable Görtler mode ( $n=200$ ) at various large amplitudes on the growth of most unstable mode with  $n=100$ .

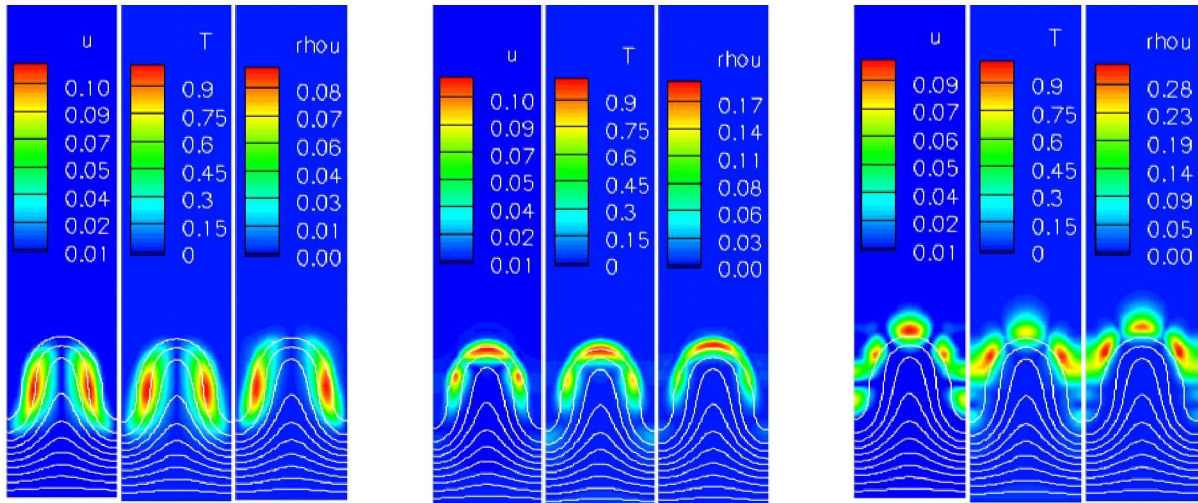


(a) N-factor evolution for fixed frequency disturbances.

(b) Spatial growth rate evolution corresponding to Fig. 2(a).

(c) Growth rate as function of disturbance frequency at  $x = 2.3$  m.

Figure 3. Secondary instability characteristics of Görtler vortices for the wind tunnel case documented in Figure (a-e).



(a) Mode 1, odd

(b) Mode 2, even

(c) Mode 3, even

Figure 4. Representative eigenfunctions for streamwise velocity perturbations associated with the three modes of secondary instability associated with the wind tunnel case documented in Figure 1 (a-e). All three modes shown above have a frequency of 53 kHz. The white lines represent the streamwise velocity contours. The eigenfunctions are normalized so that peak temperature perturbation is equal to unity.

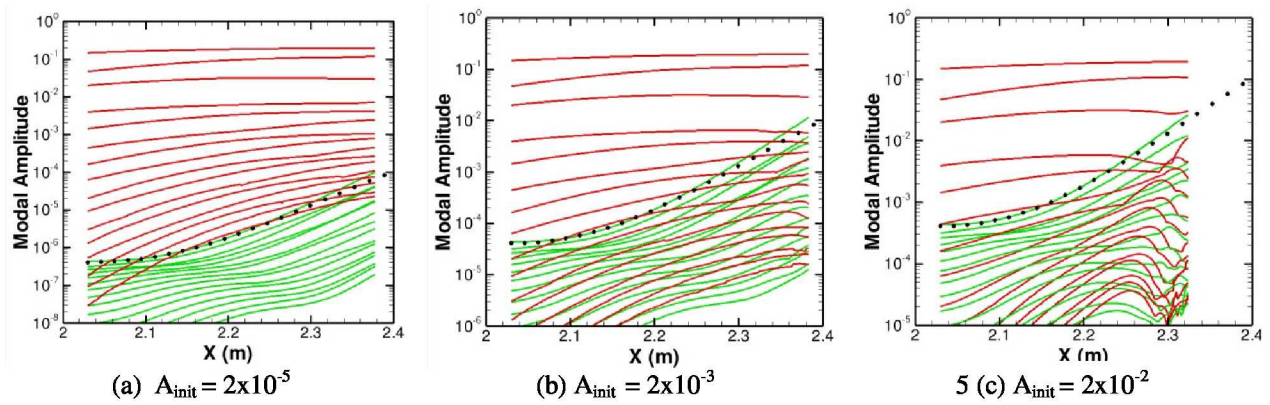


Figure 5 Streamwise velocity modal amplitudes of stationary Görtler vortex modes (red lines) and unsteady secondary instability modes of 52.5 kHz in frequency (green lines). Different lines present the amplitudes of modes with different spanwise wave numbers. The black dots present the amplitude predicted by linear secondary instability theory. ( $A_{init}$  indicates the initial amplitude of temperature fluctuation associated with the secondary instability mode).

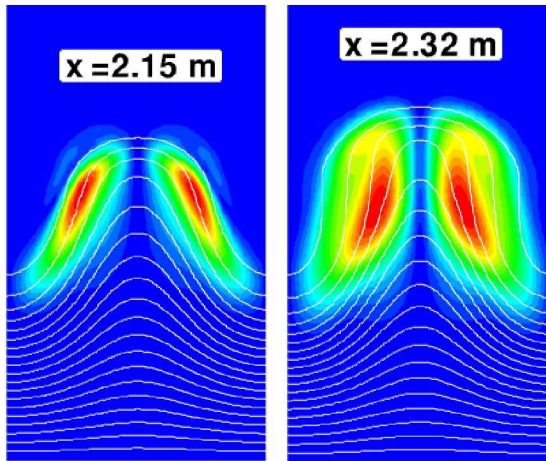


Figure 6. RMS contours of streamwise velocity of secondary instability of 52.5 kHz in fundamental frequency. The back ground white lines present the time averaged streamwise velocity contours.

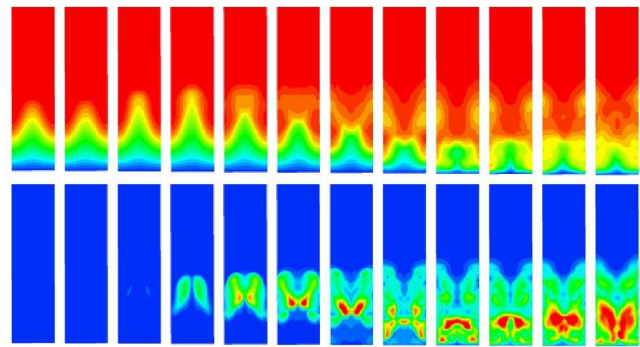


Figure 7. DNS results of mean (top) and RMS (bottom) contours of streamwise velocity in various streamwise planes with  $x$  increasing from left to right. Strong growth of secondary instability eventually destroys the bell structure of Görtler vortices and leads to breakdown.

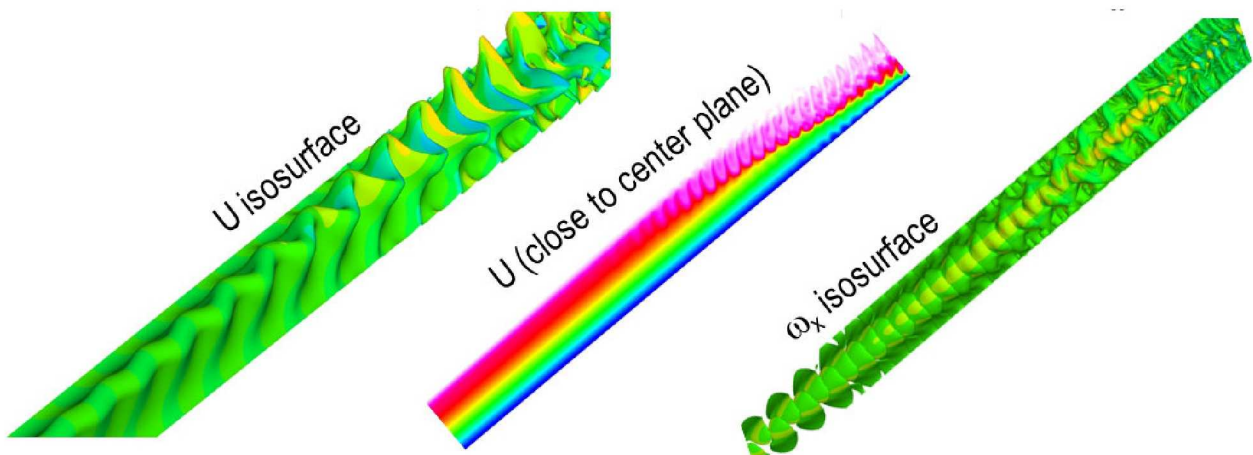


Figure 8. Left: iso-surface of streamwise velocity; center: streamwise velocity contours close to center plane; right: iso-surface of streamwise vorticity.

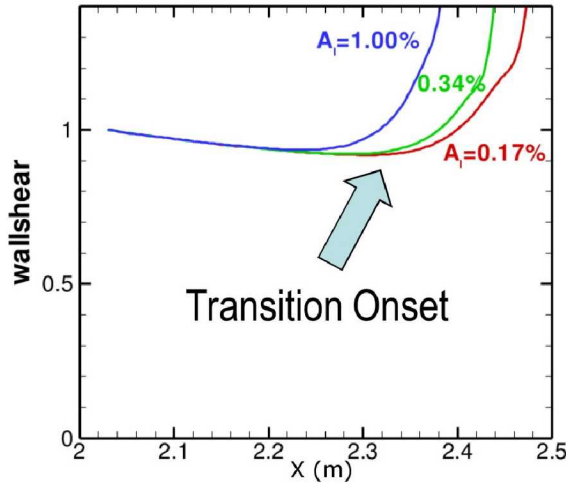


Figure 9. Wall shear for various secondary instability initial amplitudes.

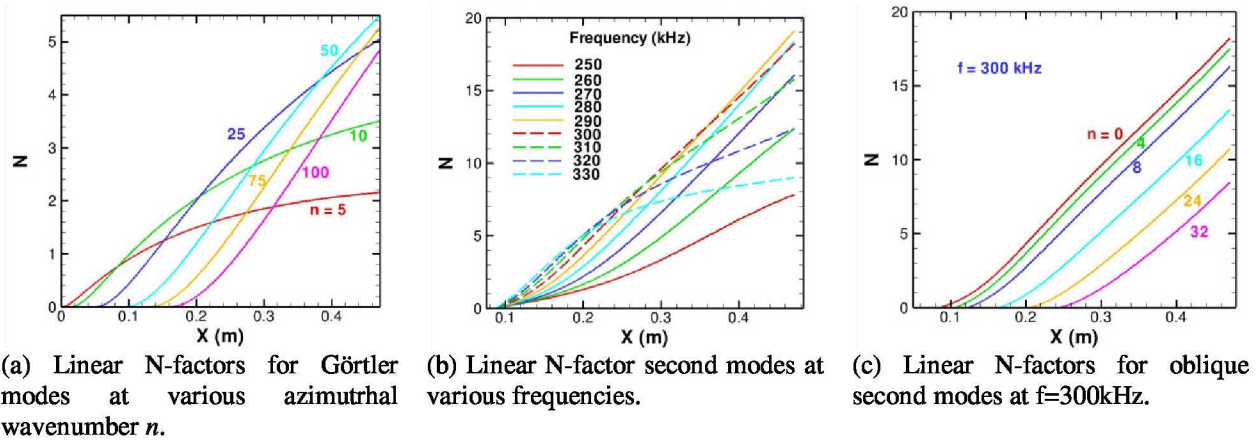


Figure 10. Linear N-factors of instability modes for the Mach 6 compression cone.

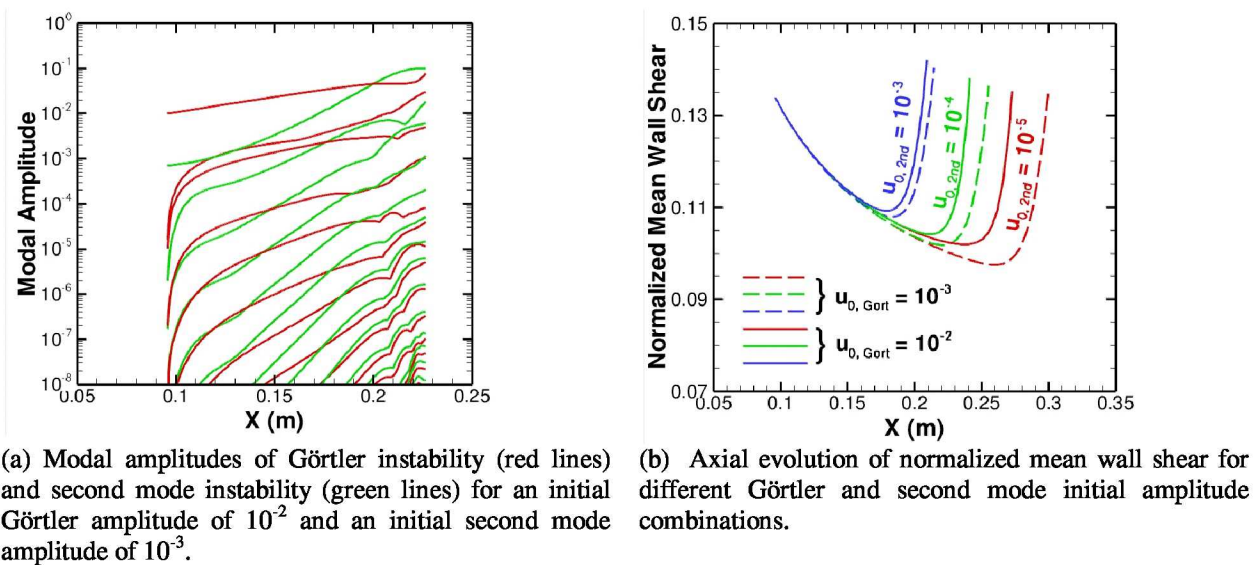


Figure 11. Co-evolution of Görtler and second mode instabilities.

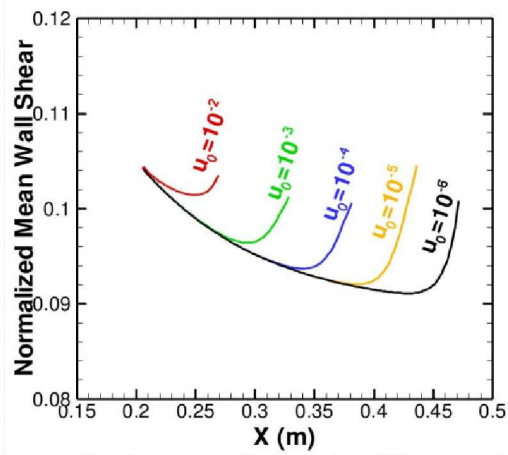


Figure 12. Axial evolution of normalized mean wall shear for different oblique second mode initial amplitudes for the interactions of two oblique waves ( $n=24$ ) of opposite azimuthal orientations.